



Published in final edited form as:

Cell Rep. 2015 February 24; 10(7): 1173–1186. doi:10.1016/j.celrep.2015.01.050.

ROCK-Isoform Specific Polarization of Macrophages Associated with Age-Related Macular Degeneration

Souska Zandi^{1,2,3,*}, Shintaro Nakao^{1,2,4,*}, Kwang-Hoon Chun⁵, Paolo Fiorina⁶, Dawei Sun^{1,2,7}, Ryoichi Arita⁴, Ming Zhao^{1,8}, Enoch Kim⁹, Olivier Schueller⁹, Stewart Campbell⁹, Mahdi Taher^{1,2}, Mark Ivan Melhorn^{1,2}, Alexander Schering^{1,2}, Francesca Gatti⁶, Sara Tezza⁶, Fang Xie^{1,2,7}, Andrea Vergani⁶, Shigeo Yoshida⁴, Keijiro Ishikawa⁴, Muneo Yamaguchi⁴, Fumiyuki Sasaki¹⁰, Ruth Schmidt-Ullrich¹¹, Yasuaki Hata⁴, Hiroshi Enaida⁴, Mitsuko Yuzawa¹², Takehiko Yokomizo¹⁰, Young-Bum Kim¹³, Paul Sweetnam⁹, Tatsuro Ishibashi⁴, and Ali Hafezi-Moghadam^{1,2}

¹Center for Excellence in Functional and Molecular Imaging, Brigham & Women's Hospital, and Department of Radiology, Harvard Medical School, Boston, MA 02115 ²Angiogenesis Laboratory, Massachusetts Eye & Ear Infirmary, and Department of Ophthalmology, Harvard Medical School, Boston, MA 02114 ³Swiss Eye Institute, Rotkreuz and Berner Augenklinik am Lindenhofspital, Department of Ophthalmology, Bern, Switzerland ⁴Department of Ophthalmology, Graduate School of Medical Sciences, Kyushu University, Fukuoka, Japan ⁵Gachon Institute of Pharmaceutical Sciences, College of Pharmacy, Gachon University, Incheon 406-799, Republic of Korea ⁶Nephrology Division, Boston Children's Hospital, Harvard Medical School, Boston, MA 02115; and Division of Transplant Medicine, San Raffaele Hospital, Milan, Italy ⁷Department of Ophthalmology, the First and Second Affiliated Hospitals of the Harbin Medical University, Harbin, China ⁸State Key Laboratory of Oncology, Minimally Invasive Interventional Division, Medical Imaging Center, Sun Yat-Sen University, Guangzhou, China ⁹Surface Logix, Inc., 50 Soldiers Field Place, Brighton, MA ¹⁰Department of Biochemistry, Juntendo University School of Medicine, Tokyo, Japan ¹¹Department of Signal Transduction in Tumor Cells, Max-Delbrück-Center for Molecular Medicine, Robert-Rössle-Str. 10, 13092 Berlin, Germany ¹²Department of Ophthalmology, School of Medical Sciences, Nihon University, Tokyo, Japan ¹³Division of Endocrinology, Diabetes and Metabolism, Beth Israel Deaconess Medical Center and Harvard Medical School, Boston, MA 02115

Abstract

Age is a major risk factor in age-related macular degeneration (AMD), but the underlying cause is unknown. We find increased Rho-associated kinase (ROCK) signaling and M2 characteristics in eyes of aged mice, revealing immune changes in aging. ROCK isoforms determine macrophage polarization into M1 and M2 subtypes. M2-like macrophages accumulated in AMD, but not in

Corresponding Author: Ali Hafezi-Moghadam, MD, PhD, Brigham and Women's Hospital, 221 Longwood Ave., Boston, MA 02115, Tel: (617) 230-8556, ahm@bwh.harvard.edu.

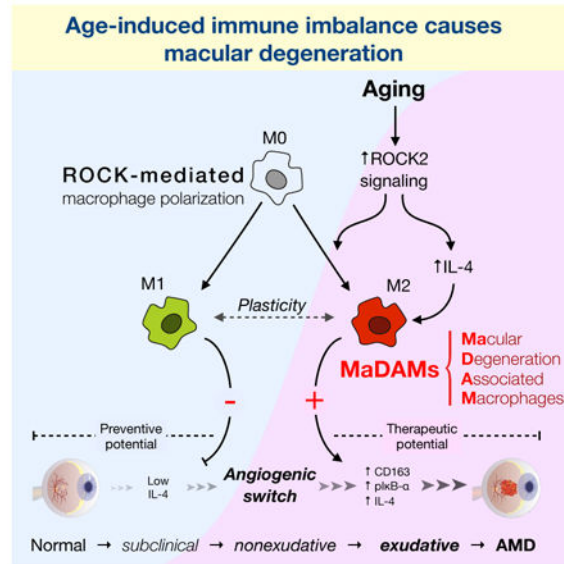
*S.Z. and S.N. contributed equally to this work.

Author Contribution Paragraph

S.Z. and S.N. performed the majority of the experiments and interpreted the results. A.H.-M. designed the study, coordinated collaborations, supervised the experimental work, and wrote the manuscript. All authors read and approved of the manuscript.

normal eyes, suggesting these macrophages may be linked to macular degeneration. M2 macrophages injected into the mouse eye exacerbated choroidal neovascular lesions, while M1 macrophages ameliorated them, supporting a causal role for macrophage subtypes in AMD. Selective ROCK2 inhibition with a small molecule decreased M2-like macrophages and choroidal neovascularization. ROCK2 inhibition upregulated M1 markers without affecting macrophage recruitment, underlining the plasticity of these macrophages. These results reveal age-induced innate immune imbalance as underlying AMD pathogenesis. Targeting macrophage plasticity opens up new possibilities for more effective AMD treatment.

Graphical Abstract



Keywords

M1/M2 differentiation; Rho kinase signaling; immune therapy; biomarker development; AMD pathogenesis

Introduction

Age-related macular degeneration (AMD) is the leading cause of adult vision loss in the developed countries. AMD has two types, the dry form that ultimately leads to macular atrophy, and the more rapidly progressing wet form, characterized by choroidal neovascularization and leakage. Most AMD cases are of the dry atrophy type, which can become exudative due to choroidal neovascularization (CNV). The normal choroid maintains quiescence through an excess of anti-versus pro-angiogenic factors. Little is known about what might reverse that balance and lead to an angiogenic switch. While aging is the strongest risk factor for AMD (Klein et al., 2002), how age influences pathogenesis is unknown. Current drug therapy in AMD is based on repeated intravitreal injections of vascular endothelial growth factor A (VEGF-A) inhibitors, which only reduces symptoms. A

recent study showed macular atrophy in virtually all long term anti-VEGF-A treated AMD cases, one third of which suffered alarming visual decay (Rofagha et al., 2013).

Macrophages are found in AMD lesions (Tsutsumi et al., 2003), however their detailed role in the disease is not understood. Plasticity and diversity are fundamental characteristics of macrophages (Sica and Mantovani, 2012). Undifferentiated M0 macrophages can polarize into classical pro-inflammatory M1-like and alternative anti-inflammatory M2-like macrophages, two extremes in a continuum of polarization states (Sica and Mantovani, 2012). A mixture of polarization phenotypes coexist, which reflect the highly dynamic and complex tissue conditions. Furthermore, polarized macrophages show a high level of plasticity in response to tissue signals. Therefore, elucidation of the mechanisms and molecules involved in macrophage polarization and plasticity may provide therapeutic avenues. Both M1- and M2-like subtypes are found in AMD (Cao et al., 2011), however their roles in the pathogenesis have not been studied. IL-1 β , IL-12, IL-23, IFN- γ , LPS, and TNF- α induce the M1-like phenotype that expresses CCL3, CCL5, CD80, CCR7, and iNOS. In contrast, IL-4, IL-10, IL-13, and TGF- β promote the M2-like phenotype that expresses CCL22, CD206, CD163, Ym 1, Fizz 1, and arginase 1 (Mantovani et al., 2004).

Rho-associated, coiled-coil-containing protein kinases (ROCKs) are involved in cytoskeletal rearrangement, contractility (Riento and Ridley, 2003), angiogenesis and inflammation (Arita et al., 2009). RhoA and RhoE are upstream of ROCK, which has two isoforms, ROCK1 and ROCK2, whose intracellular localizations differ depending on the type and condition of the examined cells (Chun et al., 2012). The role of ROCK isoforms in macrophage polarization and AMD is completely unexplored. ROCK substrates include myosin light chain (MLC), myosin binding subunit of myosin phosphatase (MYPT), and ezrin/radixin/moesin (ERM) proteins, while downstream targets include I κ B- α and NF- κ B (Cammarano and Minden, 2001).

Here we uncover a molecular switch for macrophage polarization through the ROCK signaling pathway. We show an M2-type shift with aging and establish the causal role of M2-like macrophages in CNV pathology.

Results

Choroidal neovascular endothelium expresses ROCK

To determine if ROCK1 and ROCK2 are expressed in human AMD, surgically excised CNV membranes from AMD patients were used for immunohistochemistry. In these samples we stained for both ROCK isoforms and for the von Willebrand Factor (vWF). Surgically excised CNV membranes from human AMD ($n=7$) and idiopathic macular degeneration ($n=7$) patients expressed high levels of both ROCK1 and ROCK2. In contrast, the retinal specimens from normal patients showed significantly less staining for either isoform ($n=5$). Analogously, in the laser-induced CNV in mouse and monkey, ROCK1 and ROCK2 co-localized in angiogenic endothelium, but were expressed far less in normal vessels (Fig. 1).

Increased ROCK signaling in choroidal neovascularization

To investigate ROCK signaling in CNV, we performed western blots for ROCK isoforms and its substrate, MYPT1, in laser-induced CNV tissues in mice. MYPT1 phosphorylation peaked at 3 and 7 days following laser injury in the mouse choroid, while ROCK1 and ROCK2 expressions remained unchanged throughout the course of CNV. To block ROCK2 activity we used a novel selective inhibitor (Supplemental Figs. 1&2). Dual ROCK1/2 and selective ROCK2 inhibition reduced pMYPT1 to normal unlasered levels (Fig. 2a).

MLC phosphorylation was increased in CNV and reduced to normal levels with dual ROCK1/2 and selective ROCK2 inhibition. Upstream of ROCK, RhoA was significantly increased in CNV, while RhoE was unchanged. Dual ROCK1/2 and selective ROCK2 inhibition reduced RhoA expression in lasered eyes to those found in unlasered controls (Fig 2b). This could suggest a feedback loop for ROCK activity in regulating RhoA.

ROCK2 inhibition reduces choroidal neovascularization and leakage

To investigate the role of ROCK in CNV, we induced CNV by laser injury and treated the mice with the dual ROCK1/2 inhibitor, fasudil, or the selective ROCK2 inhibitor and quantified lesion size and vascular leakage. CNV lesions were ~60% smaller with dual ROCK1/2 inhibition compared to control. Selective ROCK2 inhibition significantly reduced CNV in a dose-dependent fashion, 66% reduction at 1mg/kg, while maximum efficacy was reached at 10mg/kg. In comparison, the CNV size in ROCK1+/-Tie1Cre mice that have reduced endothelial ROCK1, did not differ from that of lasered Tie1Cre or WT control (Fig. 2c).

Dual ROCK1/2 and selective ROCK2 inhibition suppressed the percentage of the clinically relevant grade IV leakage (Fig. 2d). In comparison, ROCK1+/-Tie1Cre showed the same amount of leakage as lasered WT mice (Fig. 2e). Furthermore, intravitreal injections of fasudil in monkeys significantly reduced the percentage of grade IV leakages, as well as CNV membrane thickness (Fig. 2f).

Endothelial NF- κ B not required for CNV formation

To study downstream mediators of ROCK, we measured I κ B- α and pI κ B- α in the eyes of normal and lasered mice with and without inhibitor treatments. I κ B- α phosphorylation peaked 3 days after laser injury, while higher levels of NF- κ B and phosphorylated NF- κ B p65 (RelA) were detected by day 3 through 14 (Fig. 3a). NF- κ B protein expression was higher in CNV, possibly due to leukocyte accumulation. Dual ROCK1/2 and selective ROCK2 inhibition reduced CNV-induced NF- κ B protein expression, as well as I κ B- α and NF κ B phosphorylations to levels found in unlasered eyes. The I κ B- α protein expression was not affected by laser injury or the various treatments (Fig. 3b). While our results are in line with the fact that I κ B- α is downstream of ROCK, I κ B- α can also be phosphorylated by other kinases.

NF- κ B contributes to angiogenesis (Tabruyn and Griffioen, 2008), but its role in CNV is not understood. In the Tie1^{-/-} mouse, which lack endothelial NF- κ B signaling (Henke et al.,

2007), CNV and leakage were the same as that in lasered WT or in the Tie1Cre control mice (Fig. 3c&d). However, ROCK2 inhibition in the Tie1^{-N} mice significantly reduced CNV.

ROCK mediated macrophage infiltration in choroidal neovascularization

Macrophage recruitment in mice peaks 3 days after laser injury (Tsutsumi et al., 2003). The number of accumulated F4/80(+) macrophages in WT mice at day 3 was significantly reduced by dual ROCK1/2, but not by selective ROCK2 inhibition (Fig. 4a). Lasered CD18^{-/-} mice showed levels of F4/80(+) cells comparable to that of unlasered WT mice, indicating that the increased accumulation is due to recruitment.

In laser-induced CNV in monkey eyes, intravitreal fasudil injection significantly reduced macrophage infiltration (Fig. 4b). Immunohistochemistry showed staining for both ROCK1 and ROCK2 isoforms in infiltrated macrophages in the CNV lesions of mouse and monkey, but not in normal control eyes (Fig. 4c).

To investigate the differential impacts of dual ROCK1/2 versus ROCK2 inhibition on leukocyte transmigration from angiogenic vessels, we developed a new imaging technique (Supplemental Fig. 3). The combination of growth-factor-induced corneal angiogenesis with *in vivo* AO labeling of leukocytes allowed visualization of leukocyte extravasation from normal and angiogenic vessels in a chemotactic gradient. In MCP-1 implanted corneas, dual ROCK1/2 inhibition suppressed leukocyte transmigration, while selective ROCK2 inhibition did not (Fig. 4d). This is supported by our finding that dual ROCK1/2 inhibition or ROCK1 knockdown affects cytoskeletal proteins, while selective ROCK2 inhibition or ROCK2 knockdown does not (Supplemental Fig. 4).

ROCK mediated macrophage polarization in choroidal neovascularization

The role of ROCK isoforms in macrophage polarization has previously not been investigated. In surgically excised membranes from AMD patients, ROCK1 and ROCK2 co-localized with CD206, expressed on M2 macrophages (Fig. 5a). CD80(+) cells expressed ROCK1 and ROCK2 in neovascular tissues from AMD patients, whereas normal eyes did not stain for CD80, CD206, or significant staining for neither ROCK isoform.

The time course of protein expression showed elevated IL-4 and CD163 levels in CNV through day 7 or day 14, respectively. CCR7 was unchanged while CD80 was moderately higher in the first three days. Further, CCR3 that was previously reported to be higher in CNV (Takeda et al., 2009) remained unchanged at the examined time points (Fig. 5b).

To characterize the kinetics of macrophage accumulation, we performed flow cytometry in normal and lasered mouse eyes during CNV development. The number of CD11b(+)CD80(+) M1-like macrophages increased on day 1 after laser injury and remained high through day 7. In the CNV model, angiogenesis starts 3 days after laser injury and peaks on day 7 (Ishibashi et al., 1987). We found a peak of CD11b(-)CD206(+) cells on day 2 post laser injury, which preceded the reported start of angiogenesis. On days 3 through 7 the percentage of CD11b(+)CD206(+) cells increased with a peak on day 7, coinciding with the maximum angiogenic response in the laser-injury model (Fig. 5c). These data show that

even though both macrophage subtypes are found in CNV development, the accumulation kinetics of the M2-like macrophages closely matches the angiogenic response.

Dual ROCK1/2 and ROCK2 inhibition substantially decreased the CD11b(+)CD206(+) M2-like population, when examined on day 7. The CD11b(+)CD206(-) cell population was reduced by dual ROCK1/2 inhibition but not by ROCK2 inhibition (Fig. 5d).

ROCK regulates macrophage polarization

To investigate the role of ROCK signaling in macrophage polarization, we stained for each isoform in macrophages (Fig. 6a). In undifferentiated M0 macrophages ROCK1 and ROCK2 were evenly distributed in the cytoplasm. In M1 macrophages, ROCK1 was concentrated in the peri-nuclear regions. In comparison, ROCK2 was distributed in the cytoplasm. The cytoplasmic distribution of ROCK2 in M1 macrophages showed unique circular areas of non-expression reminiscent of vacuoles. In M2 macrophages, ROCK1 was evenly distributed in the cytoplasm, while ROCK2 was highly concentrated near the nucleus.

To elucidate the role of ROCK in macrophage fate, we used genetic knockdown and pharmacological inhibition (Fig. 6b). In M0 cells ROCK2 knockdown increased CCL3, while ROCK1 knockdown increased CCL22. In an M1 environment, ROCK2 inhibition decreased IL-10 secretion, while it increased CCL5. In an M2 environment, ROCK1 knockdown increased CCL22 secretion. Both dual ROCK1/2 and selective ROCK2 inhibition reduced IL-10 secretion. Furthermore, dual ROCK1/2 and selective ROCK2 inhibition reduced the percentage of CD206(+) cells in flow cytometry, while ROCK2 inhibition increased the percentage of CD80(+) cells.

In bone marrow derived M2 macrophages, dual ROCK1/2 and selective ROCK2 inhibition reduced Fizz 1 and Ym 1. In comparison, only ROCK2 inhibition but not dual ROCK1/2 inhibition reduced arginase 1. In contrast, ROCK2 inhibition significantly increased iNOS expression in RT-PCR. These data indicate a previously unknown regulatory role for ROCK isoforms in macrophage polarization.

Pharmacologic inhibition of ROCK or knockdown of ROCK isoforms did not affect VEGF-A expression (Supplemental Fig. 5).

Causal role of M2-macrophages in choroidal neovascularization

To examine the contribution of macrophage subtypes in CNV formation, we differentiated murine bone marrow-derived macrophages into M1 or M2 phenotype (Supplemental Fig. 6) and injected them into the vitreous of laser treated WT mice. While undifferentiated macrophages did not affect CNV, M2 macrophages increased the lesion size, not however in ROCK2 inhibitor treated animals. In comparison, M1 macrophages reduced CNV lesions. Intravitreal injection of M1 macrophages in lasered mice that were treated with the ROCK2 inhibitor did not reduce lesion size any further, indicating that the beneficial effect of ROCK2 inhibition in vivo is indeed through macrophage polarization (Fig. 7a).

Next, WT animals were intravitreally injected with M1 (INF- γ and LPS) or M2 (IL-4, IL-10, and IL-13) transforming cytokine cocktails. Intravitreal injection of INF- γ and LPS

reduced CNV size and leakage. CNV and leakage in the M1-cytokine cocktail injected eyes remained unaffected when the animals were in addition ROCK2 inhibitor treated.

In contrast, intravitreal injection of IL-4, IL-10, and IL-13 increased CNV size and the percentage of clinically relevant IV leakage, which were reduced to control levels when the animals were in addition ROCK2 inhibitor treated (Fig. 7b&c). These results indicate the importance of the cytokine profile in CNV, mediated through ROCK signaling.

M2-skewed IL-12p40^{-/-} mice showed larger CNV lesions than WT animals. In contrast, M1-skewed adiponectin^{-/-} mice had smaller CNV lesions than WT. These results show that an endogenous bias for macrophage subtypes affects CNV. While ROCK2 inhibition significantly reduced CNV size in IL-12p40^{-/-} mice, it did not do the same in adiponectin^{-/-} mice (Fig. 7d). The efficacy of ROCK2 inhibition in IL-12p40^{-/-} mice and lack of it in adiponectin^{-/-} mice further supports the finding that the beneficial effects of ROCK2 inhibition are through a shift in macrophage polarization.

Age compounded ROCK signaling and an M2 shift

To investigate ROCK signaling as a function of age, we quantified ROCK isoforms, their downstream mediators, and macrophage markers in the choroids of young (8–12 week old) and aged (>16 month old) WT mice with and without laser injury. Compared to the baseline in the normal young MYPT1- and I κ B- α phosphorylation were higher in the lasered young and in the normal aged animals, with the highest levels found in the aged lasered animals, suggesting a compounding effect of age. In comparison, MYPT1 and I κ B- α protein expressions did not differ between the groups (Fig. 7e).

IL-4 was elevated in the young WT animals with CNV compared to the base levels in the normal young eyes. Unlasered aged WT mice had higher IL-4 levels compared to young WT animals even with CNV. Interestingly, the highest IL-4 level was found in the unlasered aged animals. CD163 was exclusively increased in CNV, while it was not affected by age in the normal eyes. The M1 specific markers CCR7 and CD80 were at similar levels in young and aged animals with or without laser injury (Fig. 7e). However, contrary to prior report (Takeda et al., 2009), CCR3 protein was unchanged in the eyes with CNV (Supplemental Fig. 7).

The higher levels of IL-4 in CNV was reversed by dual ROCK1/2 or selective ROCK2 inhibition. ROCK2 inhibition but not dual ROCK1/2 inhibition increased the M1 markers CD80 and CCR7 in lasered eyes (Fig. 7f).

Discussion

We introduce ROCK signaling as a master switch in macrophage polarization and suggest that M2-like macular-degeneration-associated macrophages (MaDAMs) are a cause of disease. Paradoxically, macrophages have been reported to promote CNV (Tsutsumi et al., 2003) and also to inhibit CNV (Apte et al., 2006), without elucidating which macrophage subtypes might be involved. Our work resolves this apparent discrepancy and illuminates how macrophages can both decrease and increase CNV, depending on their phenotype.

When injected into the vitreal cavity, M1-like macrophages reduced, while M2-like macrophages increased CNV. While both cell types were found in laser-injured mouse choroids, the accumulation kinetics of M2-like macrophages match the angiogenic response. Smaller CNV lesions in M1-skewed adiponectin^{-/-} mice, in contrast to the larger lesions in the M2-skewed IL-12p40^{-/-} mice, further bolstered the key role for macrophage polarization in CNV. ROCK2 inhibition suppressed M2- and furthered M1 polarization, while, ROCK1 inhibition furthered M2 polarization.

In mouse, monkey, and human, ROCK expression and signaling were associated with CNV. In human AMD membranes, angiogenic but not normal vessels expressed ROCK isoforms, making them candidate biomarker. Phosphorylation of downstream mediators of ROCK - MLC, MYPT1, I κ B- α , and NF- κ B p65 - were increased in CNV and suppressed with dual ROCK1/2 or selective ROCK2 inhibition, indicating a key role for this pathway in CNV. NF- κ B protein expression was higher in CNV, possibly due to immune cell accumulation. While we excluded a role for endothelial NF- κ B in CNV, NF- κ B activity in immune cells could be decisive in AMD. Dual ROCK1/2 and selective ROCK2 inhibition significantly reduced CNV, albeit through different mechanisms. We found ROCK1 signaling to be required for macrophage extravasation, while ROCK2 inhibition did not affect recruitment. Upstream of ROCK, RhoA was increased in CNV and reduced to normal levels with ROCK inhibition.

So-called MaDAMs accumulate in AMD, possibly due to changes in the chorioretinal microenvironment with age. A potential cause could be IL-4, which we found increased with age. ROCK2 inhibition reduced IL-4 to baseline levels in CNV, thereby affecting the cytokine microenvironment in which macrophages differentiate in addition to directly shifting the macrophage balance from M2 to M1. Interestingly, IL-4 was reported to suppress laser-induced CNV through release of soluble Flt-1 from macrophages (Wu et al., 2011), pointing out the potential of macrophage polarization and plasticity as therapeutic targets.

Analogous to tumor-associated macrophages (TAMs) that correlate with poor prognosis in cancer, MaDAMs could predict onset or severity of AMD, for instance if quantified by molecular imaging (Sun et al., 2014) or in the peripheral blood. Specifically, CD163 was only found in CNV, which could become a biomarker for exudative AMD. MaDAMs expressed both ROCK isoforms and ROCK2 inhibition reduced their number in CNV, without affecting total macrophage numbers. Selective ROCK2 but not dual ROCK1/2 inhibition increased M1 markers, CD80 and CCR7. This preserves the beneficial macrophages that are essential for retinal health (London et al., 2011) and simultaneously restores the balance between pro-angiogenic MaDAMs and their angiostatic counterparts.

Age increased ROCK signaling and the M2-type immune response, evidenced by elevated pMYPT1, pI κ B- α , CCR3, and IL-4 in the choroids of senescent mice. In contrast, age did not affect the M1-type response. This establishes a novel link between age and macrophage polarization that could explain the angiogenic switch in AMD. In contrast to prior work, in which IL-10-treated macrophages failed to reduce CNV (Kelly et al., 2007), our results showed that M2-differentiated macrophages significantly increase CNV. Importantly, the

mechanism shown in this work is distinct from the prior concept of differential recruitment of macrophage subtypes in CNV (Zhao et al., 2013), since ROCK2 does not affect macrophage recruitment.

Demand is high for a ROCK2 specific inhibitor (Riento and Ridley, 2003). This study introduces an orally available selective ROCK2 inhibitor, which lacks toxicity in human. The antagonistic role of ROCK isoforms in macrophage polarization suggests that more efficacy and fewer side effects is possible with isoform specific inhibition. A benefit of selective ROCK2 inhibition compared to dual ROCK1/2 inhibition is the M1 upregulation in lesions, since selective ROCK2 inhibition does not interfere with macrophage recruitment. Instead, by targeting macrophage plasticity, selective ROCK2 inhibition restores the immunological balance that prevails in the normal young eye. Compared to anti-VEGF-A agents that only treat late symptoms (Rofagha et al., 2013), targeting macrophage polarization addresses roots of the disease.

AMD is considered an inflammatory disease (Hollyfield et al., 2008), yet our results highlight its immune-modulatory nature. We found elevated NF- κ B signaling in CNV that was suppressed with ROCK inhibition. NF- κ B can be pro- or anti-angiogenic (Aurora et al., 2010). Since CNV was independent of endothelial NF- κ B activity, yet pI κ B- α was higher in aging and CNV, it is feasible that NF- κ B's contribution to CNV is in immune cells. The causal role of macrophage polarization in CNV challenges the paradigm that AMD is inflammatory. Instead, rather than a sole phenotypic signature or a cell type, our results point toward immune imbalance as a root of AMD. These insights together with the considerable plasticity of macrophages open new prospects for immune-based therapy in age-related diseases. While macrophage polarization is a promising target, the complexity of the subject matter requires future insights to be fully understood.

This study introduces the role of ROCK in macrophage polarization. Aging increases ROCK2 signaling, resulting in overt expression of the pro-angiogenic MaDAMs. This newly revealed chain of events explain the angiogenic switch in the aging eye. In contrast, a shift of the fundus microenvironment towards M1, *i.e.* through selective ROCK2 inhibition, reduces the pathology and restores the physiological macrophage balance found in the young. These results facilitate the development of biomarkers for AMD and new immune based therapies.

Materials & Methods

Human tissues

Human CNV membranes were surgically excised from AMD and idiopathic neovascular maculopathy patients. The symptoms were documented as classic CNV, subfoveal or juxtafoveal CNV with hemorrhage and retinal detachment, when present. Average age for AMD patients ($n=7$) was 71.3 years, and for idiopathic neovascular maculopathy ($n=7$) 33.2 years. Average duration from the time of onset to surgery, 8.9 months. Average size of the CNV lesions, 0.84 of the disc diameter. Control eyes were from donor eyes without AMD. An institutional review board granted approval for allocation and histological analysis of specimens.

Animals

All animal experiments adhered to The Guiding Principles in the Care and Use of Animals (DHEW Publication, NIH 80-23).

Monkeys—Eyes from cynomolgus monkeys between 3 and 4 years of age were used in this study. General anesthesia was achieved by intramuscular injection of ketamine hydrochloride (20mg/kg, Sankyo Yell Pharmaceutical Products Co).

Rodents—Male C57BL/6J mice (Stock# 000664; Jackson Laboratories), weighing 24–28g. Jackson Laboratory tested and confirmed that their C57BL/6J production line is free of the *rd8* mutation. In addition, we tested the *rd8* status of our experimental mice by PCR, the results of which showed that our experimental strains were free of the *rd8* mutation in the *Crb1* gene (Mattapallil et al., 2012) (Supplemental Fig. 8). The genetically modified mice used in this work were phenotypically normal and on C57BL/6J background. They did not differ in weight or age from their WT counter parts. Animals were sheltered in ventilated plastic cages in a temperature-controlled animal facility with a 12-hour light/dark cycle and were fed standard laboratory chow and water *ad libitum*. In this study, young WT were 8–12 weeks old, while aged animals were >16 months old. Male, 8–12 week old adiponectin^{-/-} and IL-12p40^{-/-} mice were purchased from Jackson labs. Adiponectin regulates M2 polarization and adiponectin^{-/-} mice express more M1 cells (Ohashi et al., 2010). Macrophages from IL-12p40^{-/-} mice have a bias toward the M2 phenotype (Bastos et al., 2002).

Tie1Cre/I κ B- α N (Tie1 N) mice: For this project, the I κ B- α N (loxP- N) mice were crossed with the Tie1Cre mice to generate the Tie1Cre/I κ B- α N mice (or short Tie1 N) that were used for CNV experiments. As a result of the I κ B- α N expression in the endothelial cells, these mice lack NF- κ B signaling in their vascular endothelium. Noteworthy, Tie-1-Cre mice do not express Cre only in the vascular endothelial cells. There was a 12–20% Cre expression in adult erythroid, myeloid and lymphoid cells (Gustafsson et al., 2001).

The I κ B- α N mice are knock-in mice. Briefly, the cDNA of the human NF- κ B suppressor I κ B- α N was integrated by homologous recombination in frame into the β -catenin locus (Schmidt-Ullrich et al., 2001). In the floxed I κ B- α N mice that were used in the current work, a loxP-stop-loxP cassette was cloned in front of the transgene, resulting in the human I κ B- α N suppressor only to be expressed in the presence of Cre (Freund et al., 2005; Henke et al., 2007; Schmidt-Ullrich et al., 2001). I κ B- α N was expressed in all tissues, consistent with the ubiquitous distribution of β -catenin.

The ROCK1^{+/-}-Tie1Cre mice: To have ROCK1 deficient mice on a pigmented background, we generated tissue specific haploinsufficient ROCK1 deficient mice on C57Bl/6J background. For this, Tie1-Cre ROCK1 LoxP^{-/-} (or endothelial-specific ROCK1-deficient mice) were generated by mating Tie1-Cre recombinase knockin mice with ROCK1 LoxP^{-/-} mice (Huang et al., 2012). Heterozygote ROCK1^{+/-} mice on C57Bl/6J background are viable and fertile with no obvious phenotypic abnormalities. They express ROCK1 in

approximately half the amount of normal WT, while there is no compensatory upregulation of ROCK2 (Rikitake et al., 2005).

Cell culture and transfection

The monocyte cell line U937 (CRL-1593.2, ATCC) was maintained in RPMI-1640 supplemented with 10% FBS (Atlanta Biologicals), glutamine (2mmol/L), penicillin (100U/mL), and streptomycin (100µg/mL; Gibco, BRL). The mouse monocyte cell line RAW 264.7 (TIB-71, ATCC) was maintained in DMEM (30-2002, ATCC).

Transfections were performed using Control- (sc-37007), ROCK1- (sc-29473h, sc-36432m) and ROCK2 (sc-29474h, sc-36433m) siRNA from Santa Cruz Biotechnology (Santa Cruz, CA, USA) via electroporation (VCA-1004 Amaxa).

Differentiation of bone marrow-derived macrophages

Bone marrow cells were collected from femurs and tibias of wild type C57Bl/6J mice. The cells were cultured in RPMI1640 medium supplemented with 20% FCS, 30% L cell sup (containing M-CSF) and P/S for 5 days. Bone marrow-derived macrophages (BMDMs) were stimulated with 1µg/ml LPS and 20ng/ml IFN- γ (M1 phenotype) or 20ng/ml IL-4, IL-10 and IL-13 (M2 phenotype) for 24 hours. BMDMs were collected and washed with PBS/2 mM EDTA (cold), incubated with 5µg/ml anti-Fc γ R mAb (2.4G2), followed by staining with 2.5µg/ml CD80-FITC, CD206-FITC, or isotype control. After washing with PBS/EDTA, BMDMs were analyzed using a flow cytometer (FACS Calibur).

Immunohistochemistry

Paraffin embedded sections of human eyes were deparaffinized and rehydrated with a graded alcohol series. Immunofluorescent staining was performed with antibodies (Abs) against human von Willebrandt factor (F3520, Sigma), human MMR (CD206, MAB2534, R&D Systems), human CD80 (ab53003 Abcam) or human ROCK1 (sc-17794, Santa Cruz Biotechnology) or ROCK2 (sc-1851, Santa Cruz Biotechnology) and identified with Alexa Fluor 488 (10µg/ml, A-11055; Invitrogen) or 647 (10µg/ml, A21244; Invitrogen) secondary Abs. On day 3 after laser injury, 10µm frozen sections of the posterior segment were prepared. The mouse eye sections were incubated with a rat anti-mouse F4/80 mAb (MCA497R, AbD Serotec) or CD11b (550282, BD Pharmingen), and subsequently with the secondary Ab. In monkey eyes, CD68 (goat pAb, sc-7082, Santa Cruz), vWF (rabbit pAb, A0082, DAKO), ROCK1 (mouse mAb, sc-17794, Santa Cruz) and ROCK2 (goat pAb, sc-1851, Santa Cruz) were stained. Images were obtained with a Leica microscope.

Western blot

To obtain tissues, animals were perfused with PBS and eyes were enucleated immediately after perfusion. Choroid-retinal pigment epithelium (RPE) complex were micro-surgically isolated and placed in 100µl of lysis buffer (mammalian cell lysis kit MCL1, Sigma), supplemented with protease and phosphatase inhibitors (P2850, P5726, P8340 Sigma), and sonicated. The lysate was centrifuged (12000rpm, 15min, 4°C) and the supernatant was collected. Each sample containing an equal amount of total protein, quantified by protein assay (Bio-Rad Laboratories), was separated by SDS-PAGE and electroblotted to PVDF

membranes (Invitrogen). To block nonspecific binding, the membranes were washed with 5% skim milk and subsequently incubated with the following: rabbit Abs against phospho-MBS/MYPT1-THr853 (CY-P1025, Cyclex), MYPT1 (sc-25618, Santa Cruz Biotechnology), phospho NF- κ B p65 (3033, Cell Signaling), NF- κ B p65 (3034, Cell Signaling), I κ B- α (9242, Cell Signaling) or mouse Abs against pI κ B- α (9246, Cell Signaling), ROCK1 and ROCK2 (611136, 610623, BD Transduction Laboratories), pERM (3149, Cell Signaling), ERM (3142, Cell Signaling), pMLC (3675, Cell Signaling), MLC (8505, Cell Signaling), IL-4 (ab11524, Abcam), CD163 (sc-33560, Santa Cruz Biotechnology), CCR3 (ab32512, Abcam), CCR7 (ab65851, Abcam), CD80 (ab53003, Abcam) and β -tubulin (ab11308, Abcam) at 4°C overnight, followed by incubation with a horseradish peroxidase-conjugated donkey or sheep Ab against rabbit or mouse IgG (NA934V, NXA931, GE Healthcare), or goat anti-rat secondary Ab (goat anti-rat IgG-HRP: sc-2032, Santa Cruz). The signals were visualized by chemiluminescence (ECL kit; GE Healthcare).

Real time RT-PCR

Total RNA from cultured RAW 264.7 cells was extracted using the RNeasy Plus Mini Kit (74134, Quiagen). 600ng cDNA per sample was synthesized with TaqMan Reverse Transcription Reagents (N808-0234, Applied Biosystems) using its contained random hexamers scaled for a reaction volume of 30 μ l. Quantitative real-time PCR was performed with the TaqMan Universal PCR Master Mix (4324018, Applied Biosystems) and the respective probes: CCL22 (Hs00171080_m1, Applied Biosystems), VEGF A (Mm01281449_m1, TaqMan), and 18S rRNA (Hs99999901_s1, Applied Biosystems) as endogenous control.

In BMDM experiments cDNA was synthesized from total RNA with Quantiscript Reverse Transcriptase and optimized blend of oligo-dT and random primers (Millipore). Gene expression was measured by the change-in-threshold (C_T) method based on quantitative real-time PCR in an Light Cycler (Roche) with SYBR Green I.

The primer sets for the murine Arg1 (Arginase-1; for, cctgaaggaactgaaaggaaag, rev, ttggcagatatgcaggagt), Retnla (Fizz1; for, ccctccactgtaacgaagactc, rev, cacaccagtagcagctatcc), Chi3l3 (Ym1; for, gaacactgagctaaaaactctctg, rev, gagaccatggcactgaacg) and Nos2 (iNOS; for, gggctgtcacggagatca, rev, ccatgatggtcacattctgc), β -Actin (Actb; For, catccgtaaacctctatgccaac, Rev, accagaggcatacagggaca) were used. Experiments were performed using Applied Biosystem's Step One Plus real-time PCR system using the company's standard cycles. The relative abundance of transcripts was normalized according to that of mouse GAPDH (4352932, Applied Biosystems), 18S rRNA.

Flow cytometry

To examine macrophages in the retina and choroid, cells were prepared from mouse eyes. To collect a sufficient number of ocular inltrating cells, 50 burns were delivered to mouse eyes by laser. After laser injury, eyes were enucleated at different time points (1, 2, 3, 5, and 7days). The anterior segment (cornea, iris, and lens) was excised and the posterior segment of the eye including sclera, choroid, and retina was disrupted with scissors and then shaken

in DMEM (plus 10% FBS (Gibco Laboratories), 100U/ml penicillin, 100µg/ml streptomycin) supplemented with 0.5mg/ml Collagenase type D (11088874103, Boehringer Mannheim) at 37°C for 60min. The supernatants were collected and passed through a mesh. After 3 washes, viable cells were obtained. A total of 12 eyes (6 individual pools) were examined per group. The cells were stained with PE anti-mouse CD11b (557397, BD Pharmingen), FITC anti-mouse CD206 (MMR, 123005; BioLegend) and PE-Cy5 anti-mouse CD80 Abs (15-0801-81, eBioscience).

RAW 264.7 cells were stained with PerCP anti-mouse CD11b (101230, BioLegend), PerCP anti-mouse F4/80 (123006, BioLegend), PE anti-mouse CD80 (12-0801, eBioscience), and FITC anti-mouse CD206 (141704, BioLegend).

Laser-induced CNV

Laser-induced CNV is a wound healing model that mimics the angiogenesis and leakage aspects of AMD (Ishibashi et al., 1987). To induce CNV, C57BL/6J mice were anesthetized and pupils were dilated with 5% phenylephrine and 0.8% tropicamide. Using a 532-nm laser (Oculight GLx, Iridex), a slit-lamp delivery system, and a cover glass as a contact lens, four spots (100mW, 50µm, 100ms) were placed in each eye. The lesions were located at 3, 6, 9 and 12 o'clock meridians centered on the optic nerve head, and 2–3 disk diameters from the optic nerve head. The same technique was used in cynomolgus monkeys (700mW, 100µm, 100ms). Development of a bubble under laser radiation confirmed the rupture of the Bruch's membrane. Eyes showing hemorrhage were excluded from experiments.

Quantification of CNV and leakage

Seven or fourteen days after laser injury, the size of CNV lesions was measured in choroidal flat mounts. Briefly, mice were anesthetized and perfused through the left ventricle with PBS, followed by 5ml of 5% fluorescein isothiocyanate-dextran (FD2000S; Sigma Aldrich) in 1% gelatin. The anterior segment and retina were removed from the eyecup. The remaining RPE-choroid-sclera complex was flat mounted, after relaxing radial incisions, using Mounting Medium (FM 100119, Thermo Scientific) and coverslips. Micrographs of the choroidal complex were taken with a Leica Microscope. The volume of the lesions was quantified, using confocal microscopy (Leica TCS SP2 laser scanning confocal microscope). The magnitude of the CNV lesions was determined by measuring the hyperfluorescent area with Openlab Software (Improvision). The grade of leakage was determined by Fluorescein angiography (FA).

Fluorescein angiography

FA was performed in anesthetized rodents, mice (C57BL/6J) and rats (Brown Norway), using a digital fundus camera (SLO; HRA2; Heidelberg Engineering), 7 and 14 days after laser injury. Fluorescein injections were performed intravenously (0.2ml of 2% fluorescein; Akorn, NDC 17478-253-10). For FA in monkeys, animals were injected with 5% fluorescein intravenously (Fluorescite, Alcon). FA images were evaluated by two masked retina specialists. The grading criteria were: Grade-I, no hyper uorescence; Grade-II, hyper uorescence without leakage; Grade-III, hyper uorescence in the early or mid-transit images and late leakage; Grade-IV, bright hyper uorescence in the transit images and late leakage

beyond the treated areas. The Grade-IV lesions were considered clinically significant (Lara-Castillo et al., 2009).

Treatments

To block both ROCK isoforms, the dual ROCK1/2 inhibitors, fasudil (20mg/kg, H-2330; LC Laboratories, MW: 364.29) and Y-27632 (10mg/kg, S1049, selleckchem.com) were administered daily by intraperitoneal injections. To block ROCK2, mice received twice daily intraperitoneal injections of the selective ROCK2 inhibitor (10mg/kg, SurfaceLogix, MW: 570.61). The ROCK2 selective inhibitor, is currently being developed for clinical use by Kadmon® (Kadmon Corporation, LLC, NY) under the designation KD025. The control animals received equivalent amounts of vehicle, glyceryl trioctanoate (91039, Sigma-Aldrich). Intravitreal injections of fasudil and ROCK2 inhibitor (5µl in rat and 1µl in mouse; 30µmol/l) were performed on day 0, 3 and 6 after CNV induction, using BSS Plus as vehicle. Adult cynomolgus monkeys received intravitreal injection of fasudil (30µM), 3 times per week.

The inhibitor treatments, unless indicated otherwise, started on day 0 at the same time as CNV induction, and continued daily (fasudil once per day, ROCK2 inhibitor twice per day) until harvest.

Statistical analysis

All values are expressed as mean±SEM. Data were analyzed by Student's *t*-test, analysis of variance (ANOVA), or chi-squared test. Differences between the experimental groups were considered statistically significant (*) or highly significant (**), when the probability value, *P* was <0.05 or <0.01, respectively.

Supplementary Material

Refer to Web version on PubMed Central for supplementary material.

Acknowledgments

We thank Sonja Frimmel, Sepideh Faez, Lola Chabtni, and Roberto Bassi for technical assistance and Rebecca Garland, for critical review of the manuscript. Randy Huang, David M. Dombkowski (Center for Regenerative Medicine and Technology, Massachusetts General Hospital) assisted with flowcytometry. We thank Professor K.C. Hayes for his commitment to mentorship.

This work was supported by National Institutes of Health (NIH)/National Institute of Diabetes and Digestive and Kidney Diseases through Diabetes Complications Consortium award 25732-30 (A.H.-M.), the BrightFocus Foundation, the Malaysian Palm Oil Board, and R01DK083567 (Y.B.K.). Grants from JSPS KAKENHI, Grant-in-Aid for Young Scientists (A) (#25713057 to SN).

Bibliography

- Apte RS, Richter J, Herndon J, Ferguson TA. Macrophages inhibit neovascularization in a murine model of age-related macular degeneration. *PLoS Med.* 2006; 3:e310. [PubMed: 16903779]
- Arita R, Hata Y, Nakao S, Kita T, Miura M, Kawahara S, Zandi S, Almulki L, Tayyari F, Shimokawa H, et al. Rho kinase inhibition by fasudil ameliorates diabetes-induced microvascular damage. *Diabetes.* 2009; 58:215–226. [PubMed: 18840783]

- Aurora AB, Biyashev D, Mirochnik Y, Zaichuk TA, Sanchez-Martinez C, Renault MA, Losordo D, Volpert OV. NF-kappaB balances vascular regression and angiogenesis via chromatin remodeling and NFAT displacement. *Blood*. 2010; 116:475–484. [PubMed: 20203265]
- Bastos KR, Alvarez JM, Marinho CR, Rizzo LV, Lima MR. Macrophages from IL-12p40-deficient mice have a bias toward the M2 activation profile. *J Leukoc Biol*. 2002; 71:271–278. [PubMed: 11818448]
- Cammarano MS, Minden A. Dbl and the Rho GTPases activate NF kappa B by I kappa B kinase (IKK)-dependent and IKK-independent pathways. *J Biol Chem*. 2001; 276:25876–25882. [PubMed: 11337492]
- Cao X, Shen D, Patel MM, Tuo J, Johnson TM, Olsen TW, Chan CC. Macrophage polarization in the maculae of age-related macular degeneration: a pilot study. *Pathol Int*. 2011; 61:528–535. [PubMed: 21884302]
- Chun KH, Araki K, Jee Y, Lee DH, Oh BC, Huang H, Park KS, Lee SW, Zabolotny JM, Kim YB. Regulation of glucose transport by ROCK1 differs from that of ROCK2 and is controlled by actin polymerization. *Endocrinology*. 2012; 153:1649–1662. [PubMed: 22355071]
- Freund C, Schmidt-Ullrich R, Baurand A, Dunger S, Schneider W, Loser P, El-Jamali A, Dietz R, Scheidereit C, Bergmann MW. Requirement of nuclear factor-kappaB in angiotensin II- and isoproterenol-induced cardiac hypertrophy in vivo. *Circulation*. 2005; 111:2319–2325. [PubMed: 15870116]
- Gustafsson E, Brakebusch C, Hietanen K, Fassler R. Tie-1-directed expression of Cre recombinase in endothelial cells of embryoid bodies and transgenic mice. *J Cell Sci*. 2001; 114:671–676. [PubMed: 11171372]
- Henke N, Schmidt-Ullrich R, Dechend R, Park JK, Qadri F, Wellner M, Obst M, Gross V, Dietz R, Luft FC, et al. Vascular endothelial cell-specific NF-kappaB suppression attenuates hypertension-induced renal damage. *Circ Res*. 2007; 101:268–276. [PubMed: 17585070]
- Hollyfield JG, Bonilha VL, Rayborn ME, Yang X, Shadrach KG, Lu L, Ufret RL, Salomon RG, Perez VL. Oxidative damage-induced inflammation initiates age-related macular degeneration. *Nat Med*. 2008; 14:194–198. [PubMed: 18223656]
- Huang H, Kong D, Byun KH, Ye C, Koda S, Lee DH, Oh BC, Lee SW, Lee B, Zabolotny JM, et al. Rho-kinase regulates energy balance by targeting hypothalamic leptin receptor signaling. *Nat Neurosci*. 2012; 15:1391–1398. [PubMed: 22941110]
- Ishibashi T, Miller H, Orr G, Sorgente N, Ryan SJ. Morphologic observations on experimental subretinal neovascularization in the monkey. *Invest Ophthalmol Vis Sci*. 1987; 28:1116–1130. [PubMed: 2439474]
- Kelly J, Ali Khan A, Yin J, Ferguson TA, Apte RS. Senescence regulates macrophage activation and angiogenic fate at sites of tissue injury in mice. *J Clin Invest*. 2007; 117:3421–3426. [PubMed: 17975672]
- Klein R, Klein BE, Tomany SC, Meuer SM, Huang GH. Ten-year incidence and progression of age-related maculopathy: The Beaver Dam eye study. *Ophthalmology*. 2002; 109:1767–1779. [PubMed: 12359593]
- Lara-Castillo N, Zandi S, Nakao S, Ito Y, Noda K, She H, Ahmed M, Frimmel S, Ablonczy Z, Hafezi-Moghadam A. Atrial natriuretic peptide reduces vascular leakage and choroidal neovascularization. *Am J Pathol*. 2009; 175:2343–2350. [PubMed: 19910509]
- London A, Itskovich E, Benhar I, Kalchenko V, Mack M, Jung S, Schwartz M. Neuroprotection and progenitor cell renewal in the injured adult murine retina requires healing monocyte-derived macrophages. *J Exp Med*. 2011; 208:23–39. [PubMed: 21220455]
- Mantovani A, Sica A, Sozzani S, Allavena P, Vecchi A, Locati M. The chemokine system in diverse forms of macrophage activation and polarization. *Trends Immunol*. 2004; 25:677–686. [PubMed: 15530839]
- Mattapallil MJ, Wawrousek EF, Chan CC, Zhao H, Roychoudhury J, Ferguson TA, Caspi RR. The Rd8 mutation of the *Crb1* gene is present in vendor lines of C57BL/6N mice and embryonic stem cells, and confounds ocular induced mutant phenotypes. *Invest Ophthalmol Vis Sci*. 2012; 53:2921–2927. [PubMed: 22447858]

- Ohashi K, Parker JL, Ouchi N, Higuchi A, Vita JA, Gokce N, Pedersen AA, Kalthoff C, Tullin S, Sams A, et al. Adiponectin promotes macrophage polarization toward an anti-inflammatory phenotype. *J Biol Chem*. 2010; 285:6153–6160. [PubMed: 20028977]
- Riento K, Ridley AJ. Rocks: multifunctional kinases in cell behaviour. *Nat Rev Mol Cell Biol*. 2003; 4:446–456. [PubMed: 12778124]
- Rikitake Y, Oyama N, Wang CY, Noma K, Satoh M, Kim HH, Liao JK. Decreased perivascular fibrosis but not cardiac hypertrophy in ROCK1+/- haploinsufficient mice. *Circulation*. 2005; 112:2959–2965. [PubMed: 16260635]
- Rofagha S, Bhisitkul RB, Boyer DS, Sadda SR, Zhang K. Seven-Year Outcomes in Ranibizumab-Treated Patients in ANCHOR, MARINA, and HORIZON: A Multicenter Cohort Study (SEVEN-UP). *Ophthalmology*. 2013
- Schmidt-Ullrich R, Aebischer T, Hulsken J, Birchmeier W, Klemm U, Scheidereit C. Requirement of NF-kappaB/Rel for the development of hair follicles and other epidermal appendices. *Development*. 2001; 128:3843–3853. [PubMed: 11585809]
- Sica A, Mantovani A. Macrophage plasticity and polarization: in vivo veritas. *J Clin Invest*. 2012; 122:787–795. [PubMed: 22378047]
- Sun D, Nakao S, Xie F, Zandi S, Bagheri A, Rezaei Kanavi M, Samiei S, Soheili ZS, Frimmel S, Zhang Z, et al. Molecular imaging reveals elevated VEGFR-2 expression in retinal capillaries in diabetes: a novel biomarker for early diagnosis. *FASEB J*. 2014
- Tabruyn SP, Griffioen AW. NF-kappa B: a new player in angiostatic therapy. *Angiogenesis*. 2008; 11:101–106. [PubMed: 18283548]
- Takeda A, Baffi JZ, Kleinman ME, Cho WG, Nozaki M, Yamada K, Kaneko H, Albuquerque RJ, Dridi S, Saito K, et al. CCR3 is a target for age-related macular degeneration diagnosis and therapy. *Nature*. 2009; 460:225–230. [PubMed: 19525930]
- Tsutsumi C, Sonoda KH, Egashira K, Qiao H, Hisatomi T, Nakao S, Ishibashi M, Charo IF, Sakamoto T, Murata T, et al. The critical role of ocular-infiltrating macrophages in the development of choroidal neovascularization. *J Leukoc Biol*. 2003; 74:25–32. [PubMed: 12832439]
- Wu, W-K.; Nicholson, LB.; Bates, DO.; Dick, AD. IL-4 Stimulates Macrophage Soluble Flt-1 Production and IL-4 Administration Inhibits Laser-induced CNV in Mice. Paper presented at: ARVO; Fort Lauderdale, FL. 2011.
- Zhao H, Roychoudhury J, Doggett TA, Apte RS, Ferguson TA. Age-dependent changes in FasL (CD95L) modulate macrophage function in a model of age-related macular degeneration. *Invest Ophthalmol Vis Sci*. 2013; 54:5321–5331. [PubMed: 23821188]

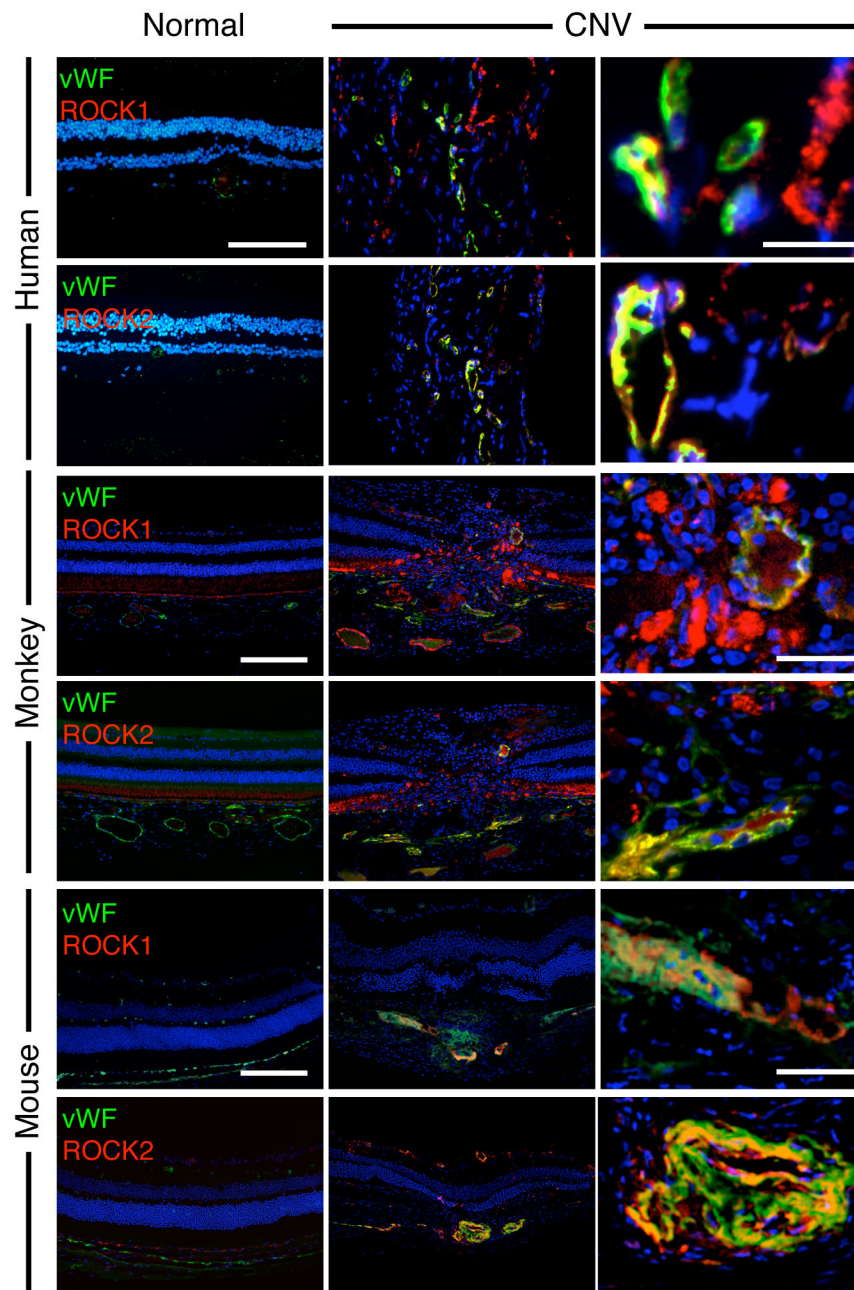


Figure 1. CNV lesions express both ROCK isoforms

Double immunostaining shows localizations of vWF (*green*) and ROCK1 or ROCK2 (*red*) in ocular tissues from normal retina-choroidal complexes and human AMD membranes, laser-induced CNV in monkey and in mice. In the CNV tissues of all three species, non-endothelial cells also expressed ROCK isoforms. Blue, nuclei stained with 4,6-diamidino-2-phenylindole (DAPI). Bar, low magnification 100µm, high magnification, 20µm.

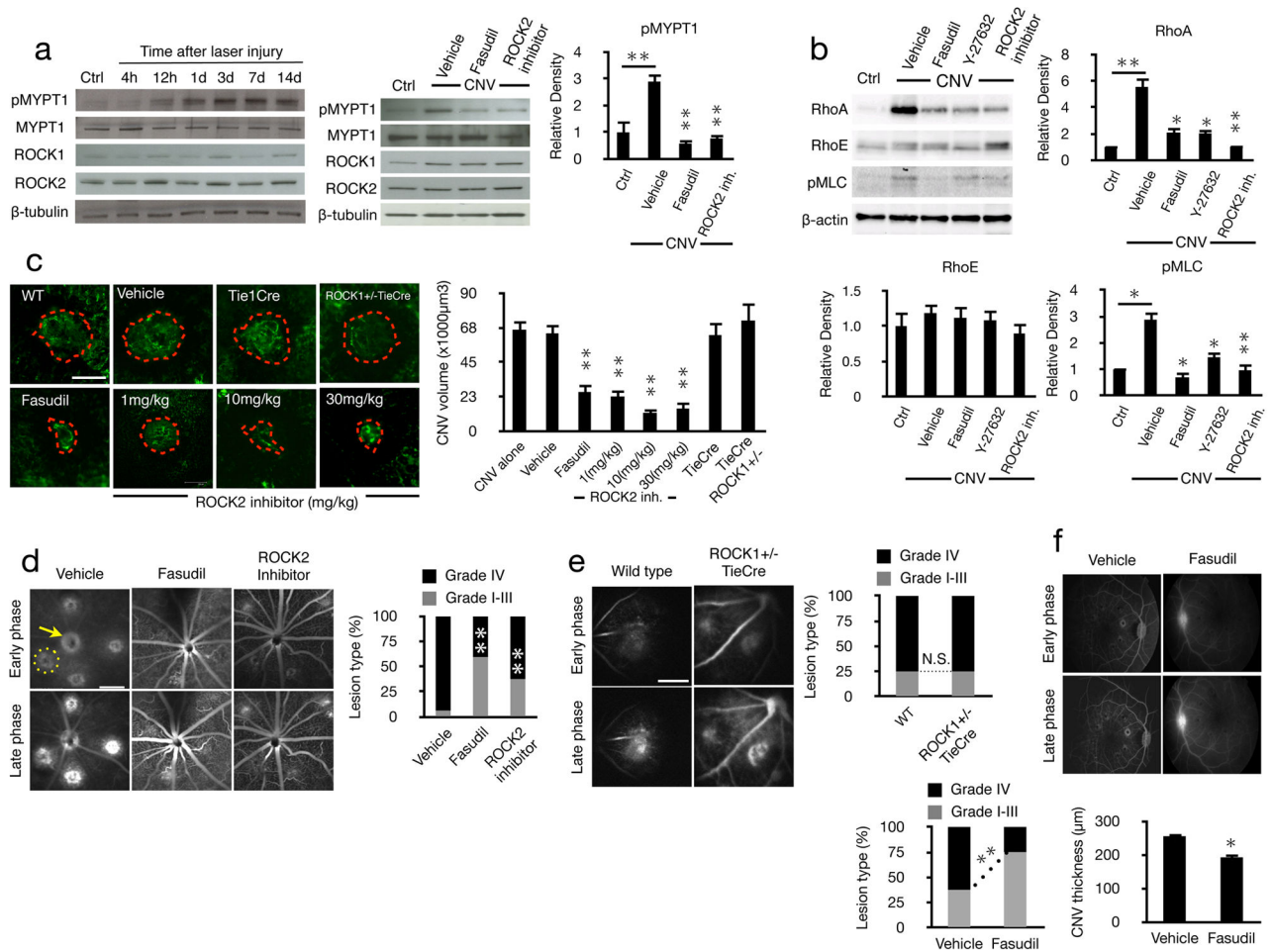


Figure 2. CNV depends on ROCK signaling

ROCK signaling was quantified in experimentally induced CNV and the effect of ROCK inhibition was studied *in vivo*. **(a)** Western blot analysis using whole cell lysates from choroids of normal and CNV eyes at the indicated time points after laser injury. Vehicle and inhibitor treated CNV eyes were screened at day 7 for anti-pMYPT1, anti-MYPT1, anti-ROCK1, anti-ROCK2, as well as **(b)** anti-RhoA, anti-RhoE, and anti-pMLC Abs, $n=3$. **(c)** Representative mouse CNV lesions treated with vehicle, fasudil ($n=5$, 40 lesions), ROCK2 inhibitor at different concentrations ($n=4$, 32 lesions in each group) and in ROCK1+/-TieCre mouse ($n=5$, 40 lesions) with the corresponding quantifications. Red dashed line, extent of the laser-induced CNV lesions filled with FITC-dextran in flatmounted choroids. Scale bar, 100 μ m. **(d)** Leakage from the angiogenic vessels was visualized by fluorescein angiography and quantified in early (1–2min) and late-phase (6–8min) angiograms of Brown Norway rats treated with vehicle, fasudil or ROCK2 inhibitor, as well as **(e)** in ROCK1+/-TieCre mice. **(f)** Fluorescent angiography in monkey and CNV thickness measurements with vehicle or fasudil treatment ($n=4$). Yellow dashed circle, extent of the CNV lesions filled with fluorescein; yellow arrow, optic nerve. Scale bar, 1mm. The percentage of lesions graded as I, II, III, defined as no to moderate leakage, and IV, clinically relevant leakage ($n=4$, 32 lesions). * $P < 0.05$; ** $P < 0.01$.

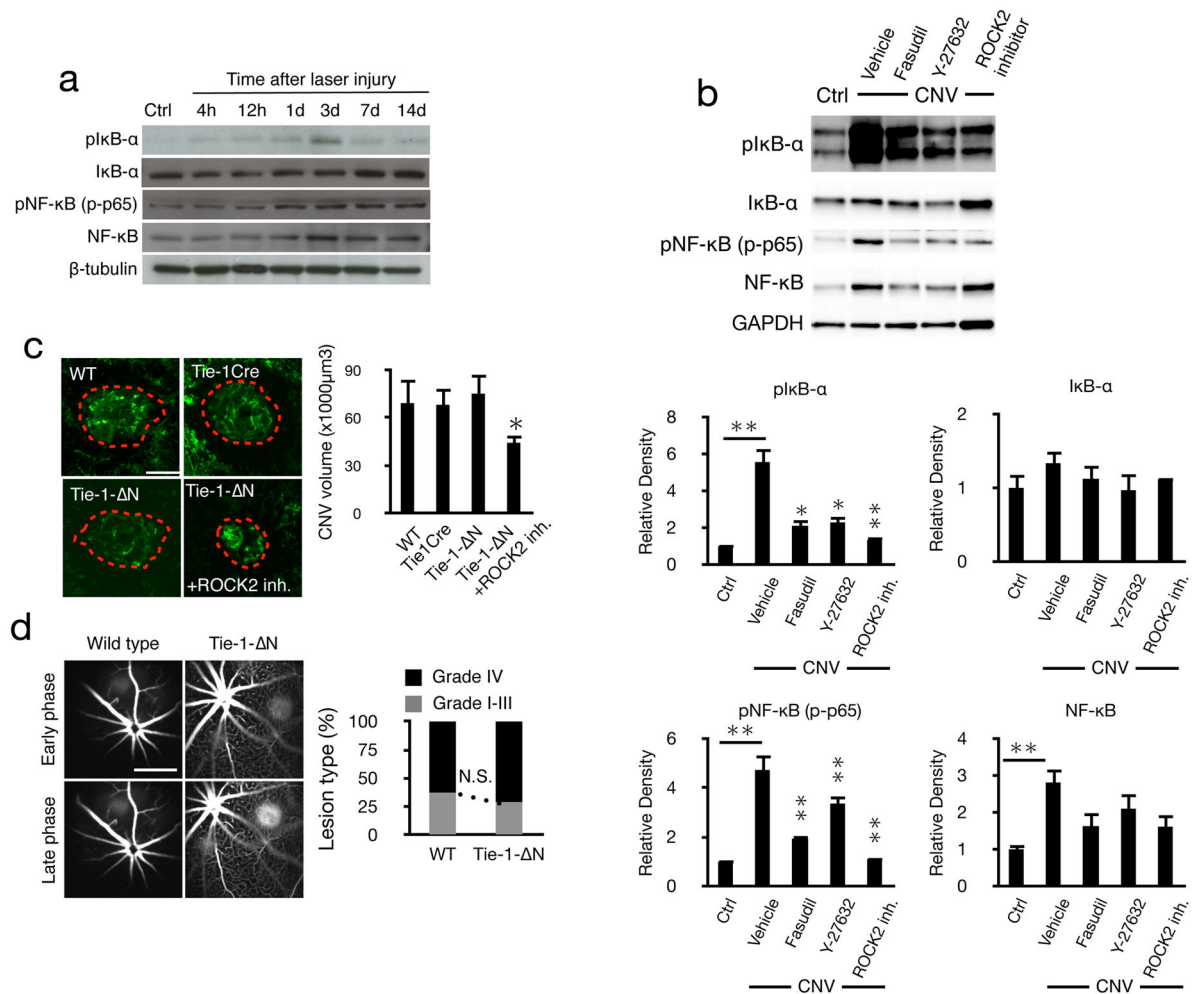


Figure 3. Lack of endothelial NF-κB signaling does not affect CNV

(a) Western blot analysis in whole cell lysates of lasered eye extracts at different time points after laser injury. (b) Representative western blot of anti-pIκB-α, anti-IκB-α, anti-pNF-κB p65, anti-NF-κB, anti-GAPDH with fasudil (20mg/kg), Y-27632 (10mg/kg) or ROCK2 inhibitor (10mg/kg) treatment in choroids with CNV (day 7) with the corresponding quantifications. (c) Representative micrographs of CNV lesions (day 7) in choroidal flat mounts from C57BL/6J, TieCre or Tie-1- N mice with or without ROCK2 inhibition. Scale bar, 100μm and quantitative analysis of CNV volume ($n=5$ animals in each group, 40 lesions). * $P < 0.05$; ** $P < 0.01$. (d) Representative early phase (1–2min) and late-phase (6–8min) fluorescein angiograms in C57BL/6J and Tie-1- N mice and quantification. Scale bar, 1mm.

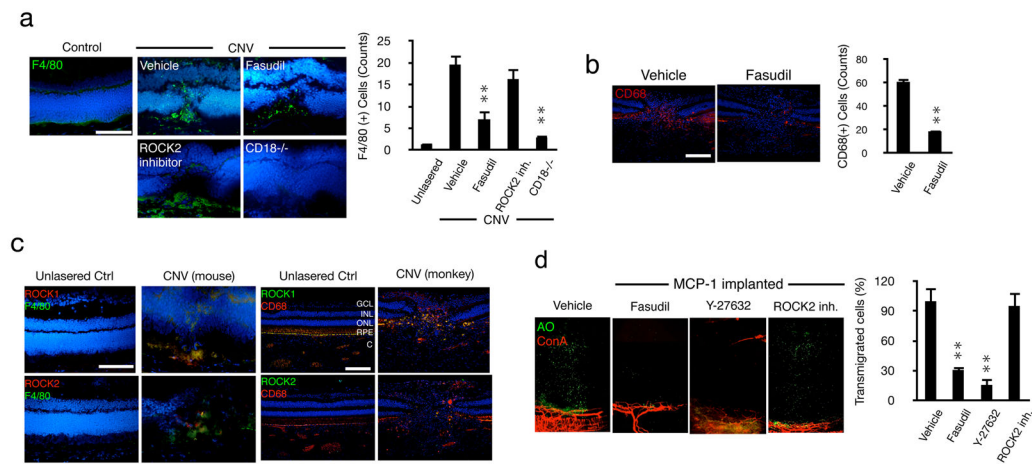


Figure 4. ROCK-mediated regulation of inflammatory leukocyte infiltration during CNV
(a) Representative micrographs of laser-induced CNV lesions, immunostained for F4/80 in C57BL/6J mice treated with vehicle, fasudil or ROCK2 inhibitor, or in *CD18*^{-/-} mice and quantification of the number of F4/80-positive macrophages in CNV lesions ($n=3$ animals in each group). In each eye 6 lesions were placed. From each lesion 10 or more sections were stained, the results of which were averaged for each lesion/animal. Scale bar, 100 μ m. **(b)** Impact of fasudil on macrophage infiltration in laser-induced CNV in monkey ($n=4$). Representative micrographs of CNV lesions, immunostained for CD68 in lasered monkeys treated with vehicle or fasudil. Quantification of the number of CD68-positive leukocytes in CNV lesions ($n=4$). ** $P < 0.01$. Scale bar, 100 μ m. **(c)** Double immunostaining of laser-induced CNV in monkey and mice with Abs of ROCK1 or ROCK2 and CD68 or F4/80. *GCL*, ganglion cell layer; *INL*, inner nuclear layer; *ONL*, outer nuclear layer; *RPE*, retinal pigmented epithelial layer; *C*, choroid. Bar, 50 μ m. **(d)** *Ex vivo* imaging of impact of ROCK inhibitors on MCP-1-mediated leukocyte transmigration. AO(+) leukocytes and Con A(+) angiogenic vessels in MCP-1-implanted corneas, 2h after AO injection, 24 hours after pellet implantation with vehicle, fasudil, Y-27632 or ROCK2 inhibitor treatment. Quantification of the number of AO(+) leukocytes in areas of MCP-1-implanted corneas 2h after AO injection, 24 hours after pellet implantation. $n=4$; * $P < 0.05$, ** $P < 0.01$.

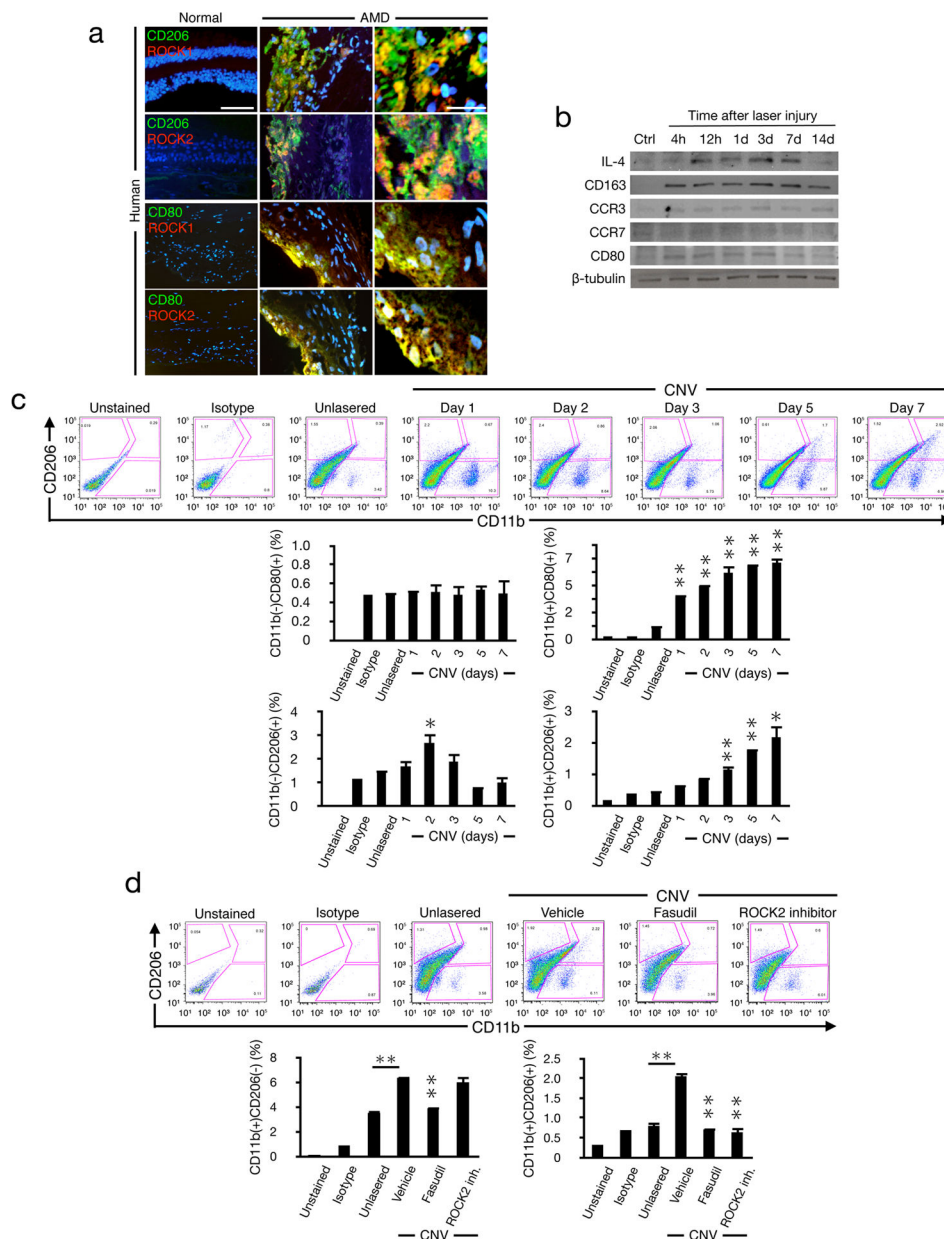


Figure 5. Polarization of ocular infiltrating macrophages by ROCK

(a) Double immunostaining of normal human retina-choroidal complex and AMD membranes with Abs against CD206 or CD80 (*green*) and ROCK1 or ROCK2 (*red*) ($n=4$). Overview bar, 50 μ m; high magnification, 20 μ m. **(b)** Western blot analysis with anti-IL-4, anti-CD163, anti-CCR3, anti-CCR7, anti-CD80 or anti- β -tubulin Abs, using whole cell lysates from lasered mouse choroids at the indicated time points after injury. Other proteins from the same experiment shown in Fig. 2a. **(c)** FACS analysis of infiltrating cells from untreated and laser-injured choroids at the different time points after laser injury. Cells were stained for CD11b, CD80, and CD206. The percentages of infiltrating CD11b(+)CD206(+), CD11b(+)CD80(+), CD11b(-)CD206(+), CD11b(-)CD80(+) cells in CNV at the indicated times ($n=6$). **(d)** FACS analysis of infiltrating cells from CNV eyes (choroid) with vehicle,

fasudil or ROCK2 inhibitor treatment at day 7 with PE-CD11b mAb and FITC-CD206 mAb. The percentages of infiltrating CD11b(+)CD206(+) cells and CD11b(+)CD206(-) cells in CNV with the treatment at day 7 ($n=6$). * $P < 0.05$; ** $P < 0.01$.

Author Manuscript

Author Manuscript

Author Manuscript

Author Manuscript

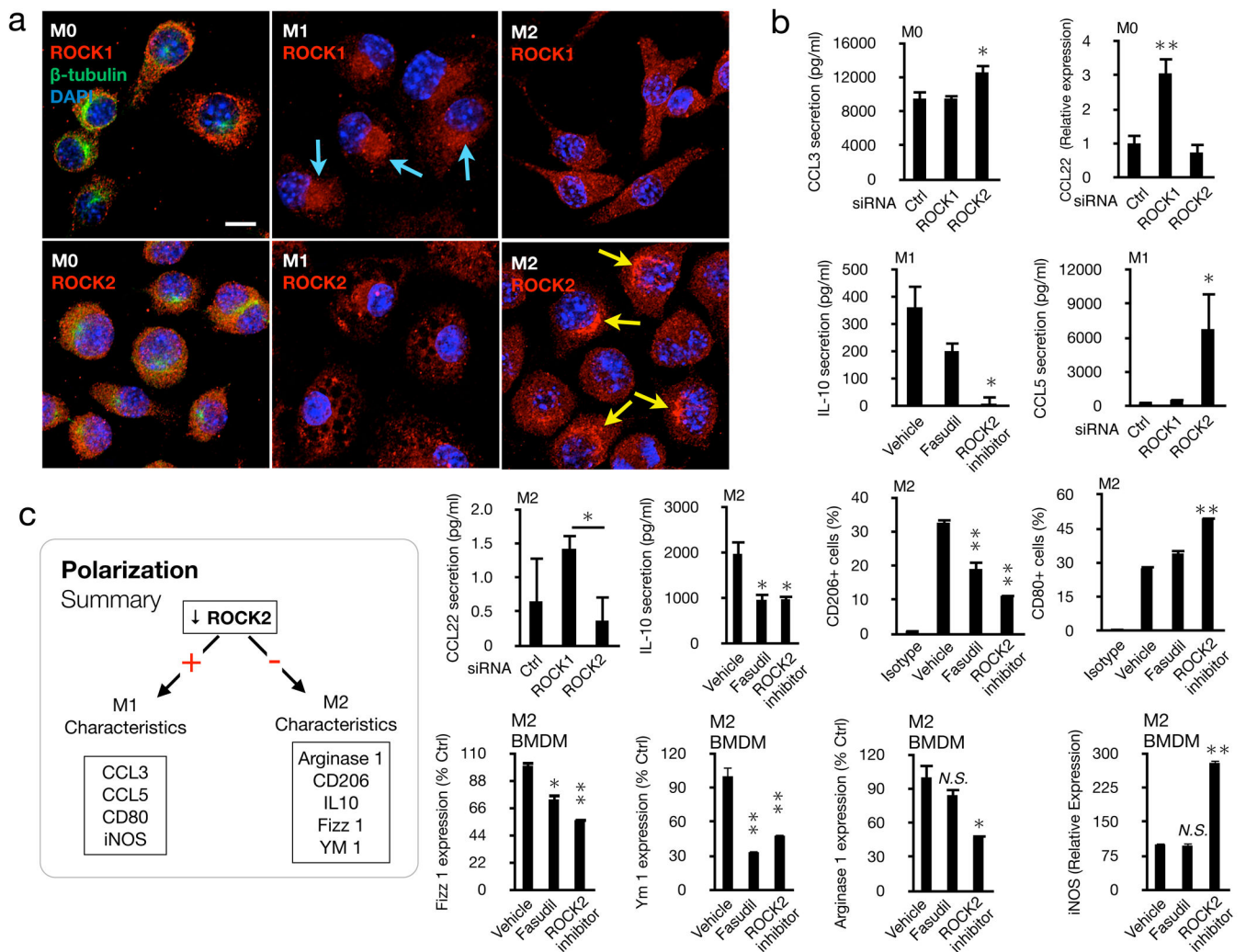


Figure 6. Isoform-specific inhibition of ROCK determines macrophage fate

(a) Cellular localization of ROCK isoforms in polarized macrophages (M0, M1, M2). RAW 264.7 cells were differentiated into M0, M1, and M2 by cytokine treatment and used for immunostaining with Abs against ROCK1 or ROCK2 (red), β -tubulin (green) and DAPI (blue). Arrowheads, vacuoles. Bar, 10 μ m. In a small number of M1 cells, ROCK2 was also found more concentrated around the nucleus. **(b)** ROCK isoforms were blocked in RAW 264.7, U937 and BMDM cells in M0-, M1-, or M2 environments. Chemokines, cell markers, and genes were quantified by luminex, flow cytometry, or rtPCR. Data represent average from three or more independent experiments. RT-PCR data was evaluated after subtraction of the specific endogenous control gene expression (18S rRNA). * $P < 0.05$; ** $P < 0.01$ **(c)** Schematic overview of how ROCK signaling impacts polarization.

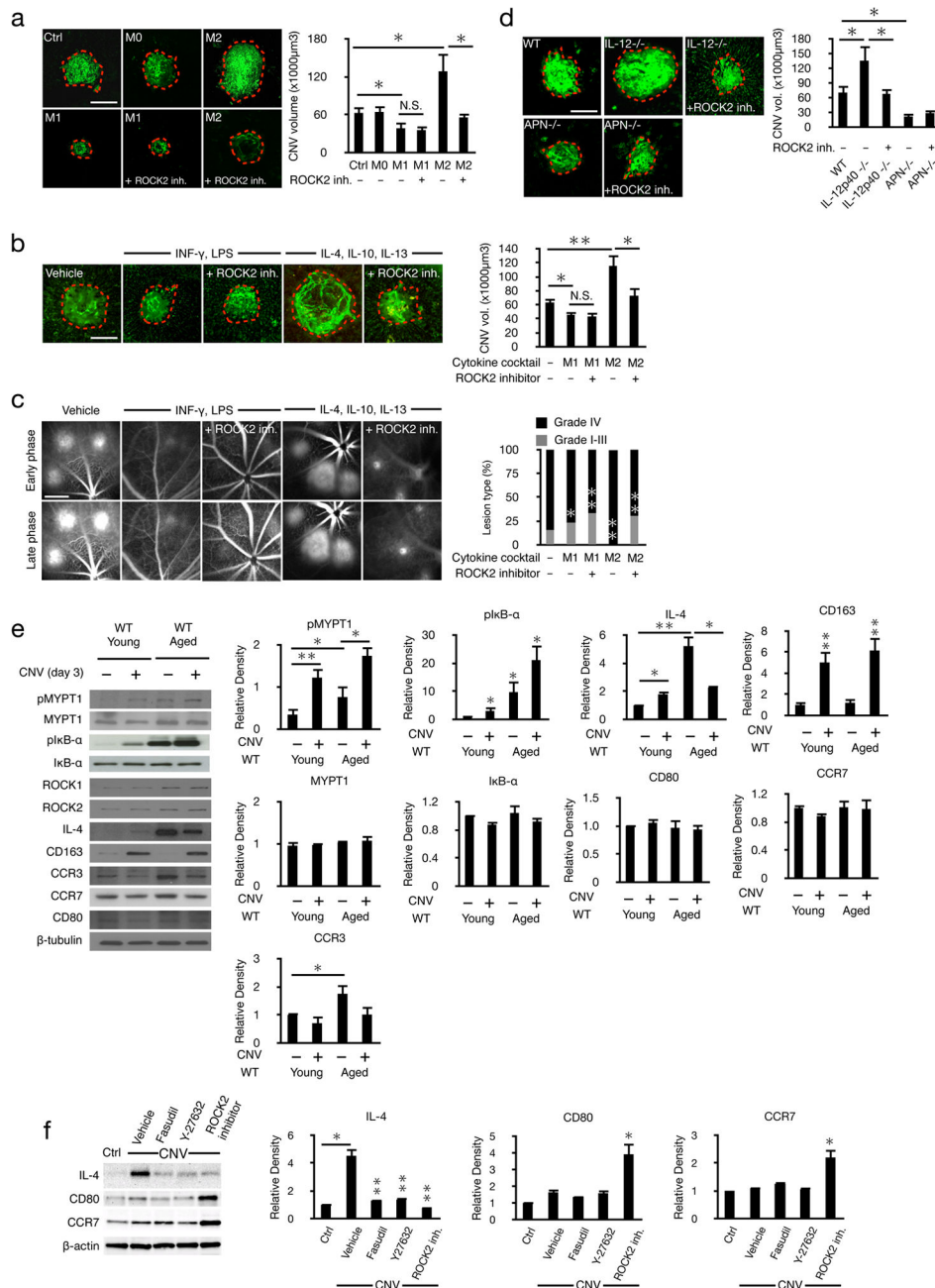


Figure 7. Age-induced ROCK-signaling and M2 differentiation cause CNV

(a) Representative laser-induced CNV results from mice after intravitreal injections of vehicle, M0, M1, or M2 macrophages with or without ROCK2 inhibitor and the corresponding quantifications ($n=5$ mice, 10 eyes). Scale bar, 100μm. (b) Representative micrographs of CNV lesions from mice after intravitreal cytokine injections, M1 cocktail: INF- γ and LPS, M2 cocktail: IL-4, IL-10, IL13 and the corresponding quantifications. Scale bar, 100μm. (c) Leakage from the angiogenic vessels was visualized by fluorescein angiography and quantified in early (1–2min) and late-phase (6–8min) angiograms of mice injected with either M1 or M2 cocktail. Scale bar, 1mm. (d) Representative micrographs of

CNV lesions from C57BL/6J mice, IL-12p40^{-/-} and Adiponectin^{-/-} mice with and without ROCK2 inhibitor and the corresponding quantifications. Scale bar, 100 μ m. (e) Representative western blots of normal and CNV (day 3) choroids from young (8–12 week old) and aged (>16 month old) WT mice with the corresponding quantifications; $n=3$, * $P < 0.05$; ** $P < 0.01$. (f) Representative western blots of anti-IL-4, anti-CD80 and anti-CCR7 with fasudil (20mg/kg), Y-27632 (10mg/kg) or ROCK2 inhibitor (10mg/kg) treatments in choroids with CNV (day 7) with the corresponding quantifications.

Author Manuscript

Author Manuscript

Author Manuscript

Author Manuscript